Semiconductor Physics, Quantum Electronics & Optoelectronics, 2009. V. 12, N 4. P. 328-338.

PACS 72.20.Ht, 72.20.Dp, 73.23.-b, 85.35.-p

Comparison of electron transport in polar materials for the models of low-density and high-density electron gas. Application to bulk GaN

V.V. Korotyeyev, G.I. Syngayivska, V.A. Kochelap and A.A. Klimov
V. Lashkaryov Institute of Semiconductor Physics, Department of Theoretical Physics, NAS of Ukraine
41, prospect Nauky, 03028 Kyiv, Ukraine; e-mail: singg@ukr.net, koroteev@ukr.net

Abstract. We analyzed the steady-state electron transport for bulk GaN in frame of two opposite approaches: the electron temperature approach that assumes a high-density electron gas and numerical single-particle Monte-Carlo method that assumes a low-density electron gas and does not take into account electron-electron (e-e) scattering. We have also presented an analytical solution of the Boltzmann transport equation based on diffusion approximation. The transport characteristics such as the drift velocity electric field, $V_d(E)$, and mean electron energy electric field, $\langle \varepsilon(E) \rangle$, have been calculated at nitrogen and room temperatures in the wide range of applied electric fields from zero fields up to runaway ones (~100 kV/cm) for both approaches. Our calculations were performed for doped semiconductor with equal impurity and electron concentrations, $N_i = n = 10^{16}\,\mathrm{cm}^{-3}$. The electron distribution functions in various ranges of applied fields have been also demonstrated. Within the range of heating applied fields 0–300 V/cm, we found a strong difference between the transport characteristics obtained by means of the balance equations (electron temperature approach) and Monte-Carlo procedure. However, the Monte-Carlo calculations and diffusion approximation show a good agreement at 77 K. Within the range of moderate fields 1–10 kV/cm at 77 K, we established that the streaming effect can occur for low-density electron gas. In spite of significant dissimilarity of a streaming-like and a shifted Maxwellian distribution functions, the calculated values of $V_d(E)$ and $\langle \varepsilon(E) \rangle$ show similar sub-linear behavior as the functions of the applied field E. In the high-field range 20–80 kV/cm, the streaming effect is broken down, and we observe practically linear behavior of both $V_d(E)$ and $\langle \varepsilon(E) \rangle$ for both approaches. At higher fields, we point out the initiation of the runaway effect.

Keywords: Monte Carlo method, gallium nitride, electron transport.

Manuscript received 24.06.09; accepted for publication 10.09.09; published online 30.10.09.

1. Introduction

As known, the basic electric properties of semiconductor structures are determined by a nonequilibrium distribution function (DF). In theory, the nonequilibrium DF, $f(\vec{p},\vec{r},t)$, can be found from the semi-classical Boltzmann transport equation:

$$\frac{\partial f}{\partial t} + \vec{\upsilon}\frac{\partial f}{\partial \vec{r}} + e\vec{E}\frac{\partial f}{\partial \vec{p}} = L_{\mathrm{lat}}[f] + L_{e-e}[f, f']. \qquad (1)$$

In nondegenerate case, L_{lat} is a linear integral operator describing electron scattering by the lattice and L_{e-e} is a bilinear integral operator describing electron-electron (e-e) scattering. Even for steady-state and uniform case, determination of the DF is a very complicated mathematical problem.

In modern literature, two limiting approaches are developed and used depending on intensity of the e-e scattering. The first approach [1, 2] is based on analytical calculations assuming a shifted Maxwellian form of DF

$$f(\vec{p}) = A\exp\left[-\frac{\varepsilon_p - \vec{V}_d\,\vec{p}}{k_B T_e}\right] \qquad (2)$$

with two parameters: the effective electron temperature, T_e, and drift velocity, V_d. This method can be valid at high electron concentration when $\tau_{e-e} << \tau_p, \tau_\varepsilon$, i.e., the interelectron collision time τ_{e-e} is much shorter than momentum, τ_p, and energy relaxation, τ_ε, times of the electron-lattice scattering. In this case, the electron subsystem has a collective momentum and energy budget. The parameters T_e and V_d can be found from momentum and energy balance equations (BEs). The momentum and energy BEs are obtained by multiplying Eq. (1) by p_z and ε_p, respectively, followed by the integration over all possible $\vec{p}$. Using this procedure in Eq. (1), the term $L_{e-e}[f, f']$ vanishes, and we obtain for spatially uniform steady-state case the set of non-linear algebraic equations for V_d and T_e:

$$eE = Q_p(V_d, T_e), \tag{3}$$

$$eEV_d = Q_e(V_d, T_e). \tag{4}$$

The explicit form of Q_p and Q_e is determined by the scattering probability of the specific scattering mechanism.

In the opposite situation of low-density electron gas, each electron has individual momentum and energy budget and generally the DF cannot be reduced to the shifted Maxwellian one. In this case, the Monte-Carlo (MC) method is widely used in the study of electron transport. The principle of a typical MC method is simulation on a computer the random trajectory of one electron in momentum space, which includes a large number of scattering events under the action of external forces. The DF can be obtained recording the number of appearance of the electron in each elementary cell of the momentum space during the simulation procedure. Having the DF, transport characteristics can be also obtained. The reader can find the details of the MC procedure and associated calculations of electron transport in nitrides in Refs. [3-10].

It is noteworthy that nitride compounds have become of great interest for applications in high-power semiconductor devices. The group-III nitride semiconductors, in particular GaN, differ from other semiconductors of $A^{III}B^{V}$ compounds that are well studied up to date. These nitrides have specific material characteristics [11]: the large optical phonon energy $\hbar\omega_{LO}$, the large energy splitting $\delta\varepsilon$ between the Γ-minimum and the lowest satellite valleys in the conduction band, and strong electron-polar-optical phonon coupling (characterized by the Frohlich constant α_F). For GaN, these quantities are equal to $\hbar\omega_{LO} = 0.092$ eV, $\delta\varepsilon = 1.4$–1.8 eV, and $\alpha_F = 0.41$, respectively.

In GaN-based semiconductor structures, the case of high-electron concentration is often realized, and, therefore, the BEs method is more actual for the description of transport properties. The nitride structures with a low electron concentration are met rarely. However, just this case shows a richer picture of transport effects. Also, the GaN-based semiconductors are mostly investigated in high-field range up to a few hundreds kV/cm, which is related with using these nitrides in high-power applications and in attempts to observe the Gunn effect [12-14]. Unfortunately, for low-concentration nitrides, the ranges of heating and moderate applied fields were investigated not so often both theoretically and experimentally. In the strong applied field, the electron-optical phonon interaction is the main scattering mechanism for nitrides, while in the weak electric field we observe an interplay of various kinds of scattering mechanisms. The detail analysis of experimental measurements of the transport characteristics in low fields can allow us to determine parameters of nitrides that describe the intensity of one or another scattering mechanism. Therefore, in our paper we mainly focus on these intervals for applied fields.

2. The model of electron transport in GaN

We studied the transport characteristics of hot electrons in a bulk GaN of the cubic modification. The applied electric field is assumed to be time independent. The doped GaN samples with equal electron and impurity concentrations 10^{16} cm^{-3} are considered.

The following scattering mechanisms are taken into account: scattering by acoustic phonons, polar optical phonons and ionized impurities in the Brooks-Herring model. The large intervalley separation in the group-III-nitride semiconductors allows us to neglect intervalley scattering in the assumed range of the electric fields. With the assumed electron concentrations, the hot-phonon effect can be also neglected; so that equilibrium optical phonon population is taken in the model. The electron band is considered to be a parabolic one.

The total scattering rate required for MC simulations is shown in Fig. 1 as a function of the electron energy at different lattice temperatures T.

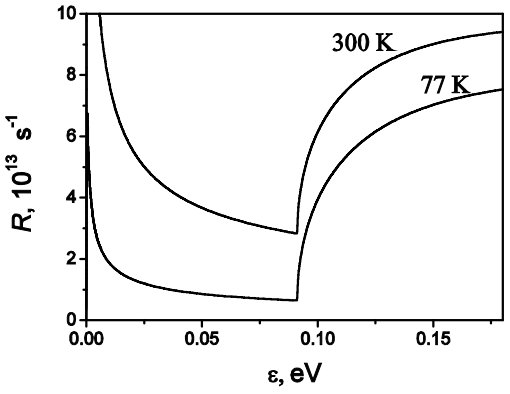

Fig. 1. Total scattering rate as a function of the electron energy in bulk GaN at 77 and 300 K.

One can see that in the "passive" energy region $(\varepsilon < \hbar\omega_{LO})$, the ionized impurity scattering dominates at 77 K. In the "active" energy region $(\varepsilon > \hbar\omega_{LO})$, the polar optical-phonon emission is always the dominant scattering. For 300 K, two scattering mechanisms, i.e., the ionized impurity scattering and the polar optical-phonon absorption are essential in the "passive" energy region.

In the frame of the model of high-density electron gas, the momentum and energy balance terms on the right-hand side of Eqs (3) and (4) are: $Q_{p,e} = Q_{p,e}^{(\mathrm{imp})} + Q_{p,e}^{(\mathrm{ac})} + Q_{p,e}^{(\mathrm{opt})}$. At the considered temperatures, the acoustic phonon and impurity scattering mechanisms are assumed to be elastic. The elastic scattering mechanism does not contribute to the electron energy balance $\left(Q_e^{(\mathrm{imp,ac})} = 0\right)$ but modifies the momentum balance. Assuming the shifted Maxwellian DF, for elastic scattering mechanisms, the function Q_p has the form:

$$Q_P = \frac{2}{V_d^2}\sqrt{\frac{2k_BT_e}{\pi m^*}}\exp\left(-\frac{m^*V_d^2}{2k_BT_e}\right)\int_0^\infty d\varepsilon \exp\left(-\frac{\varepsilon}{k_BT_e}\right)R(\varepsilon)\times$$
$$\times\left[\frac{\sqrt{\frac{m^*V_d^2}{2}}\varepsilon}{k_BT_e}\cosh\left(\frac{2\sqrt{\frac{m^*V_d^2}{2}}\varepsilon}{k_BT_e}\right)-\frac{1}{2}\sinh\left(\frac{2\sqrt{\frac{m^*V_d^2}{2}}\varepsilon}{k_BT_e}\right)\right]. \quad (5)$$

In Eq. (5), $R(\varepsilon)=\frac{1}{\tau_p^{(\mathrm{ac})}(\varepsilon)}+\frac{1}{\tau_p^{(\mathrm{imp})}(\varepsilon)}$ is determined by the sum of momentum relaxation rates for ionized impurity and acoustic phonon scattering, respectively. For example, for electron-phonon scattering via deformation potential, we use $\frac{1}{\tau_p^{(\mathrm{ac})}} = \frac{\sqrt{2}D^2k_BTm^{*3/2}}{\pi\hbar^4C_l}\varepsilon^{1/2}$ (m^* is the electron effective mass, D is the deformation potential constant, C_l is the elastic constant); for electron-ionized impurity scattering, we use $\frac{1}{\tau_p^{(\mathrm{imp})}} = \frac{\pi e^4N_i}{k_0^2\sqrt{2m^*}}\varepsilon^{-3/2}\left[\ln(1+\alpha\varepsilon)-\frac{\alpha\varepsilon}{1+\alpha\varepsilon}\right]$ (k_0 is the low-frequency permittivity, N_i is the impurity concentration. The screening parameter is given by $\alpha = 8m^*r_D^2/\hbar^2$, where r_D is the Debay radius) [15]. The specific expressions for $Q_{p,e}^{(\mathrm{op})}$ calculated for the parabolic electron dispersion law can be found in [16].

3. Transport characteristics of electrons

In this section, we will describe the specific properties of the mean kinetic characteristics $V_d(E)$ and $\langle\varepsilon(E)\rangle$. We start with consideration of the case of heating electric fields. Then, we will discuss peculiarities of electron motion in moderate fields and analyze kinetic properties of electrons in high electric fields.

3.1. Heating electric fields

In the case of high electron concentrations, the range of slightly heating electric fields is determined by the condition that T_e is close to the lattice temperature T. For the low-concentration case, conditionally, we determine the range of heating electric fields where the DF has still a small anisotropy along the applied field. The assumption of the small anisotropy of the DF allows to solve the Boltzmann transport equation analytically using the well-known diffusion approximation. Following the standard scheme [17], the DF can be expanded as

$$f(\vec{p}) = \sum_{l=0}^{\infty} f_l(\varepsilon_p)\,P_l(\cos\beta), \quad (6)$$

where $f_l(\varepsilon_p)$ is the l-th moment in the expansion of the DF, $P_l(\cos\beta)$ are the Legendre polynomials with β being the angle between the electron momentum $\vec{p}$ and the electric field $\vec{E}$. Neglecting the high-order moments with $l \geq 2$, the Boltzmann transport equation is reduced to the set of two differential equations for the two first moments f_0 and f_1. The diffusion approximation implies that $f_0 >> f_1$. For the parabolic dispersion law of electrons these equations become:

$$\frac{eE}{3\varepsilon}\sqrt{\frac{2\varepsilon}{m^*}}\frac{d(\varepsilon f_1)}{d\varepsilon} = L_{\mathrm{ac}}[f_0] + L_{\mathrm{op}}[f_0],$$
$$f_1 = -eE\sqrt{\frac{2\varepsilon}{m^*}}R(\varepsilon)^{-1}\frac{df_0}{d\varepsilon}, \quad (7)$$

where the differential operator $L_{\mathrm{ac}}[f_0]$ describes the electron energy relaxation due to acoustic phonon scattering and is of the Fokker-Plank shape:

$$L_{\mathrm{ac}}[f_0] = \frac{\delta}{\tau_p^{(\mathrm{ac})}}\frac{1}{\varepsilon}\frac{d}{d\varepsilon}\left[\varepsilon^2\left(f_0 + k_BT\frac{df_0}{d\varepsilon}\right)\right], \quad (8)$$

here δ is quasi-elasticity factor which is small at considered temperatures. The operator of polar optical phonon scattering $L_{\mathrm{op}}[f_0]$ has the form of an algebraic expression with shifted arguments:

$$L_{\mathrm{op}}[f_0] = (N_0+1)\left[\frac{f_0(\varepsilon+\hbar\omega_{LO})}{\tau^{\mathrm{op+}}(\varepsilon+\hbar\omega_{LO})} - \theta(\varepsilon-\hbar\omega_{LO})\frac{f_0(\varepsilon)}{\tau^{\mathrm{op+}}(\varepsilon)}\right] +$$
$$+ N_0\left[\frac{f_0(\varepsilon-\hbar\omega_{LO})}{\tau^{\mathrm{op-}}(\varepsilon-\hbar\omega_{LO})} - \theta(\varepsilon-\hbar\omega_{LO})\frac{f_0(\varepsilon)}{\tau^{\mathrm{op-}}(\varepsilon)}\right]. \quad (9)$$

In Eq. (9), the first term describes emission of optical phonons, while the second term corresponds to absorption of optical phonons. The phonon population is given by $N_0 = \left(\exp\left(\frac{\hbar\omega_{LO}}{k_B T} \right) - 1 \right)^{-1}$ and the scattering rates are expressed as

$$\frac{1}{\tau^{op\pm}} = \frac{e^2 \omega_{LO} \sqrt{m^*}}{\sqrt{2}\hbar} \left(\frac{1}{k_\infty} - \frac{1}{k_0} \right) \frac{1}{\sqrt{\varepsilon}} \ln \left| \frac{\sqrt{\varepsilon} + \sqrt{\varepsilon \mp \hbar\omega_{LO}}}{\sqrt{\varepsilon} - \sqrt{\varepsilon \mp \hbar\omega_{LO}}} \right|$$

(the plus/minus correspond to emission/absorption optical phonon processes, respectively). At the nitrogen temperature, we can omit the absorption term which is proportional to N_0, $N_0 << 1$.

Based on Eqs (7), we can find the isotropic part f_0 and anisotropic part f_1 of the DF. Having determined $f_0(\varepsilon)$ and $f_1(\varepsilon)$, we can calculate the mean electron energy and electron drift velocity for a given applied field:

$$\langle \varepsilon \rangle = \int_0^\infty d\varepsilon\, \varepsilon^{3/2} f_0(\varepsilon) / \int_0^\infty d\varepsilon\, \varepsilon^{1/2} f_0(\varepsilon),$$
$$V_d = \frac{1}{3} \sqrt{\frac{2}{m^*}} \int_0^\infty d\varepsilon\, \varepsilon f_1(\varepsilon) / \int_0^\infty d\varepsilon\, \varepsilon^{1/2} f_0(\varepsilon). \qquad (10)$$

The results of calculations of the transport characteristics for $T = 77$ K are shown in Figs 2a,b and 3a for the following three different approaches: MC, BEs-method, and diffusion approximation.

It is clear that in the low-density case $V_d(E)$ shows the following different behavior. In the range of very low-field, we observe the first Ohmic region. The first Ohmic region is depicted in the insert to Fig. 2a. It should be noted that the diffusion approach and the BEs one give different mobilities for the same scattering mechanisms. This peculiarity has been noted in Ref. [1] (see also Appendix). In the case of low-density electron gas, the deviation from Ohmic law takes place for the fields smaller than those in the case of high-density

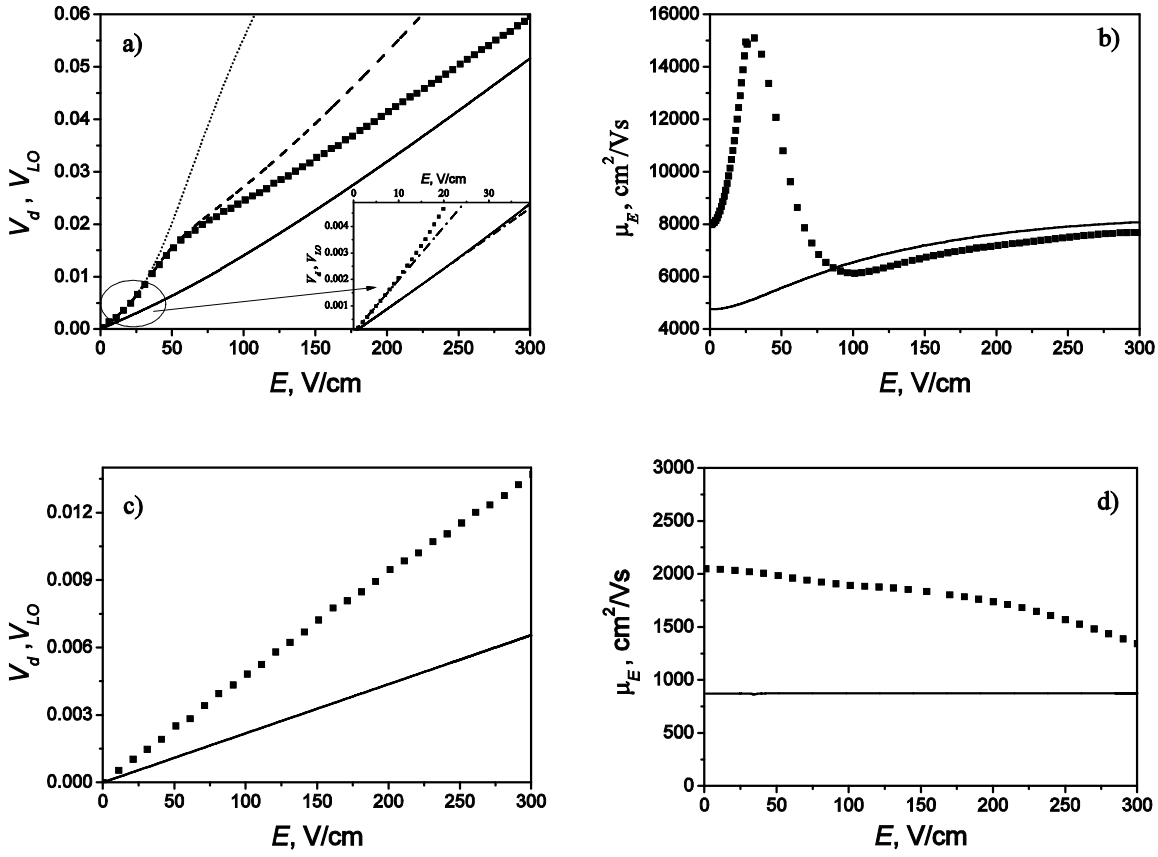

Fig. 2. Panels a) and c) present the dependence of the drift velocity on the applied field for GaN at 77 and 300 K, respectively. Doted curve in panel a) is the result of the diffusion approximation without optical phonon scattering, dash line is the same with optical phonon scattering, square dots are the results of MC simulation and solid line is the result of the BEs approach. In the insert, the dash-dot line is Ohmic behavior of $V_d(E)$ with mobilities $\mu = 8000$ and 4800 cm^2/Vs. The drift velocity is scaled to units of $V_{LO} = \sqrt{\frac{2\hbar\omega_{LO}}{m^*}}$. For GaN $V_{LO} = 4\times10^7$ cm/s. Panels b) and d) present the dependence of the differential mobility on the applied field at 77 and 300 K, respectively.

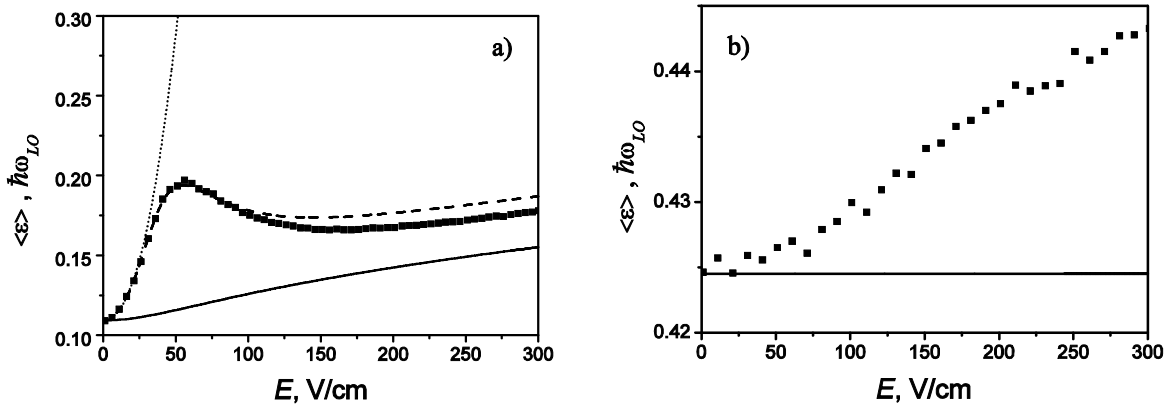

Fig. 3. Panels a) and b) present the dependence of the mean electron energy on the applied field for GaN at 77 and 300 K, respectively. Dotted curve is $\langle\varepsilon(E)\rangle$ in diffusion approximation without optical phonon scattering, dash line is the same with optical phonon scattering, square dots are the results of MC simulation and solid line presents $\langle\varepsilon(E)\rangle$ in the BEs approach. The electron energy is scaled to the energy of optical phonons $\hbar\omega_{LO}$ = 91.2 meV = 1060 K.

electron gas. In slightly higher fields than Ohmic range, both the drift velocity $V_d(E)$ and the mean electron energy $\langle\varepsilon(E)\rangle$ (Fig. 3) demonstrate a superlinear rapid growth with increasing E.

Within the interval of these fields the acoustic phonon and ionized impurity scatterings are dominating (dotted curve and square dots are almost coincide). The rapid heating of the electron gas takes place here, because the electrons can not efficiently transfer their energy to the lattice by means of quasi-elastic scattering mechanism.

Subsequent growth of the average electron energy is prevented by the mechanism of the non-elastic emission of the optical phonons. The "turn on" of the electron-optical phonon scattering is clear visible on the transport characteristics. The function $V_d(\varepsilon)$ has an inflection point and change the style from superlinear behavior to the linear one. Such a characteristic as the differential mobility, $\mu_E = \dfrac{dV_d(E)}{dE}$, is even more sensitive to the influence of the optical phonon scattering (square dots in Fig. 2b). The appearance of non-elastic scattering mechanism can be simply identified from non-monotonic behavior of μ_E. At 77 K, the electron-optical phonon interaction is turned on at 50 V/cm. At higher fields (>100 V/cm), we observe the so-called "second Ohmic" region [18]. In the case of the "second Ohmic" region, the main mechanism of electron energy relaxation is emission of polar optical phonons. At the same time, the electron momentum relaxation is related with ionized impurities. This range of the applied field is characterized by a linear dependence of $V_d(E)$ and weak decay of $\langle\varepsilon(E)\rangle$ [19]. In conditions of the "second Ohmic" region, the DF is practically isotropic ($f_0 >> f_1$) in the whole passive region except for a high-energy region bordering with active region, where $f_0 \sim f_1$. Note, the weak divergence of the transport characteristics in Figs 2 and 3 with increasing electric field, which obtained by MC-method and diffusion approximation, is explained by the violation of the condition $f_0 >> f_1$. In that time, the transport characteristics of BEs approach have not visible peculiarities. The $V_d(E)$ is practically linear and $\langle\varepsilon(E)\rangle$ shows a weak monotonic growth.

The results of calculations of the transport characteristics at 300 K by using two approaches (MC-calculation and method of BEs) are represented in Figs 2c,d and 3b. The main difference between the room temperature and nitrogen temperature cases is the presence of intensive non-elastic scattering in the passive region. At room temperature, the electron gas is practically equilibrium within the range 0-300 V/cm. The $V_d(E)$ shows a trivial Ohmic dependence for both models of the low-density electron gas and high-density electron gas. At 300 K mobilities are lower than at 77 K. The mean electron energy is practically constant and determined by lattice temperature.

3.2. Moderate electric fields

In semiconductors with strong electron-polar optical phonon interaction at low temperature ($k_BT << \hbar\omega_{LO}$) and low electron concentrations, the appropriate conditions are realized for the observation of the so-called streaming effect. The streaming effect is associated with the formation of a special type of the electron transport. In the streaming regime, the electron motion becomes almost periodic in momentum space. During one period, an electron accelerates quasi-ballistically until it reaches the critical velocity V_{LO}. Then, the electron practically instantly loses its energy

by emitting an optical phonon and starts the next period of acceleration. During this motion in the passive region, the DF strongly elongated along the electric field is established. Under streaming conditions the diffusion approximation cannot be applied to solve the Boltzmann equation, because all the moments $f_l(\varepsilon)$ are of the same order. To describe the streaming-like transport, the only MC approach is suitable. The strong inequality of scattering times in passive and active $\left(\tau_p, \tau^{\text{op}-} >> \tau^{\text{op}+}\right)$ region is also significant requirement to observe the streaming effect. The physical properties of high-quality GaN structures allow to satisfy all the streaming conditions.

A series of papers on the MC calculations of the streaming effect in GaN have been published in past decade [20, 21]. This kind of works focused on calculations of both stationary and non-stationary transport characteristics of electron gas under streaming-like condition in GaN. There are several features that can serve as an evidence of the streaming effect. The first one is the tendency to saturation of the dependences $V_d(E)$ and $\langle \varepsilon(E) \rangle$ with saturated value $V_{LO}/2$ and $\hbar\omega_{LO}/3$, respectively. The second one is the appearance of the dynamic negative differential conductivity (DNDC) in narrow region of the high frequency spectrum. The second feature is important for practical applications such as microwave generators in THz frequency range. In Ref. [21], it was shown that high electron concentrations (strong e-e scattering) and high temperatures destroy the streaming-like electron motion and prevent the appearance of DNDC. In sufficiently high electric fields, the streaming effect also disappears due to deep penetration of electrons into the active region. The previous investigations predicted that maximum values of the DNDC are obtained in range 1-10 kV/cm at low temperature, at electron concentrations about 10^{16} cm^{-3}. We performed calculations of the drift velocity and the average energy in such a range of the applied electric field by means of the MC approach and the BEs one (Figs 4 and 5). As it is clear from figures, at room temperatures the streaming is not formed. The drift velocity shows a weak sublinearity for both approaches but does not reach the characteristic streaming velocity $V_{LO}/2$. The average energy is practically constant. The situation is changed at the nitrogen temperatures dramatically. The drift velocity obtained by MC simulations has a streaming-like behavior with a quasi-saturation interval slightly below $V_{LO}/2$. At the same time, the differential mobility shows the decay behavior with tendency to saturation (Fig. 4b). Surprisingly, the BEs approach that requires a strong e-e scattering and shifted Maxwellian DF result in the similar behavior of average transport characteristics. The dependence $V_d(E)$ is also saturated, but in contrast to the room temperature results, this one lies slightly above the MC-curve. In fields higher than 6 kV/cm at 77 K, there is no visible difference between the curves $\mu_E(E)$ and between the curves $\langle \varepsilon(E) \rangle$ obtained by MC simulation and BEs approach.

From our results, it is clear that the steady-state transport characteristics in the range of streaming fields are not very sensitive to the intensity of electron–electron scattering. At the same time, another effect to be attendant to the streaming, i.e., the appearance of DNDC, is strongly dependent on the electron concentration (Ref. [21]). Thus, we can claim that the quasi-saturation behavior of $V_d(E)$ and $\langle \varepsilon(E) \rangle$ are not the distinctive signature of the streaming effect, but the effect of the DNDC is associated with streaming motion of electrons.

In spite of the likeness between the transport characteristics for both considered approaches in the range of streaming fields, the electron DFs are essentially different (see section IV).

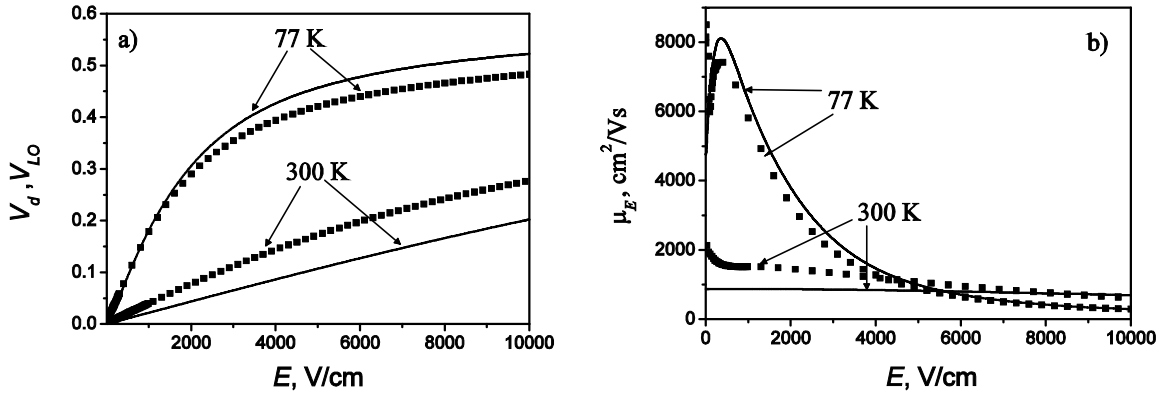

Fig. 4. Panel a) presents the dependence of the drift velocity on the applied field for GaN at 77 and 300 K. Square dots are the results of MC simulation and solid line are the results of the BEs approach. Panel b) presents the dependence of the differential mobility on the applied field.

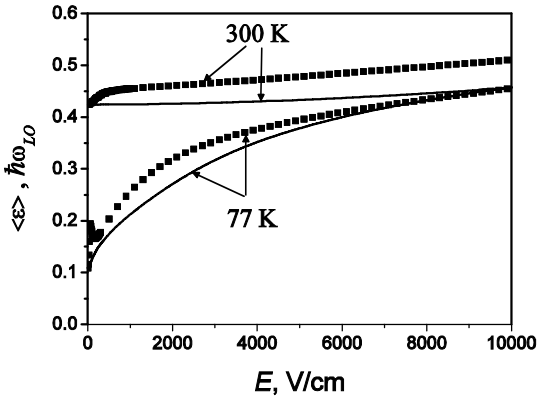

Fig. 5. Dependence of the mean electron energy on the applied field for GaN at 77 and 300 K. Square dots are the results of MC simulation and solid line indicates the results of the BEs approach.

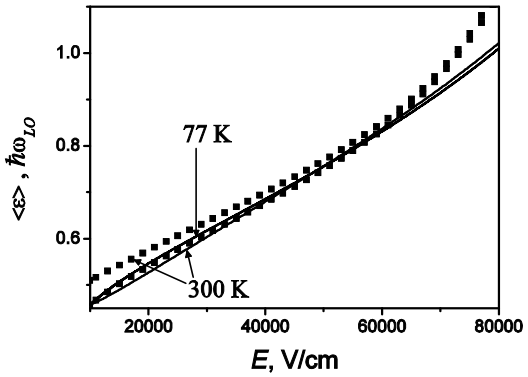

Fig. 7. The dependence of the mean electron energy on the applied field for GaN at 77 and 300 K. The line styles are the same as in Fig. 3.

3.3. The range of high electric field

Conditionally, we named the range 10-80 kV/cm for GaN as high electric fields. In conventional III-V material, such fields are associated with the Gunn effect. In nitrides, the carriers still occupy the lowest conduction valley due to the large energy distance to the neighbor valley as well as to the strong electron-polar optical interaction.

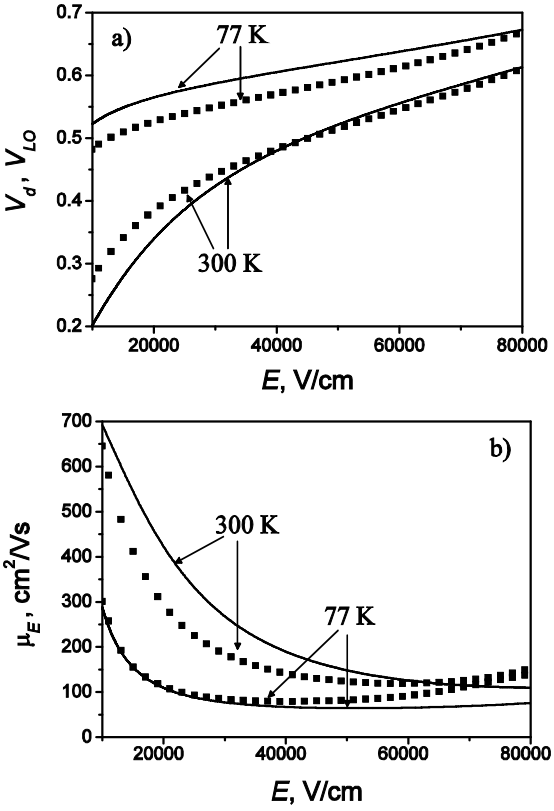

Fig. 6. Panel a) presents the dependence of the drift velocity on the applied field for GaN at 77 and 300 K. The line styles are the same as in Fig. 4. Panel b) presents the dependence of the differential mobility on the applied field.

However, in this range of applied fields the electron heating is considerable, and the mean electron energy is of the order of the optical phonon energy (Fig. 7). Both approximations give us the same behavior of $\langle \varepsilon(E) \rangle$ at 77 and 300 K. In the fields 20-50 kV/cm, the deep penetration of electrons into the active region breaks down the streaming effect even at 77 K. Instead of the quasi-saturation, we observe a linear growth of $V_d(E)$.

In fields higher than 50 kV/cm, the drift velocity as well as the average energy show the weak superlinearity (Fig. 6a,b). Apparently, this behavior is related to the onset of the runaway effect. The BEs approach predicts the onset of runaway at higher fields of about 130 kV/cm.

4. Distribution functions

All distinguishes of the transport regimes in various ranges of the applied fields for these two considered above transport models can be clearly seen from analysis of the DF. In general, the distribution function of 3D electrons is the function of three variables $p_{\|}, p_1, p_2$. In our case, the DF has an axial symmetry and therefore, it is sufficient to analyze longitudinal and transverse distributions: $N_{\|}(p_{\|}) = \int dp_1 dp_2 f(p_{\|}, p_1, p_2)$ and $N_1(p_1) = \int dp_{\|} dp_2 f(p_{\|}, p_1, p_2)$. The former determines the density probability to find an electron in the interval $dp_{\|}$ along the direction field. The latter is the same for an electron in the interval dp_1 transverse to the applied field.

$N_{\|}^{(MC)}(p_{\|})$ and $N_1^{(MC)}(p_1)$ obtained by the MC-approach at different magnitudes of the applied electric field are shown in Fig. 8 by thick lines. The same quantities obtained by the BEs approach, assuming the shifted Maxwellian form of DF are:

$$N_{\|}^{(B)}(p_{\|}) = \frac{1}{\sqrt{2\pi m^* k_B T_e}} \exp\left(-\frac{(p_{\|} - m^* V_d)^2}{2m^* k_B T_e} \right),$$

$$N_1^{(B)}(p_1) = \frac{1}{\sqrt{2\pi m^* k_B T_e}} \exp\left(-\frac{{p_1}^2}{2m^* k_B T_e} \right).$$ The latter are shown in Fig. 8 by thin lines. All DFs are normalized on the unity.

In the range of heating applied fields, for instance at 50 V/cm, the transverse and longitudinal distribution functions practically coincide for both approaches. It proves that in the range of heating fields the DF is quasi-isotropic. Also, one can see that the DF is localized in the passive region. However, for the model of the low-density gas, the tails of the DF are more advanced in higher-energy region than in the model of high-density gas. This fact illustrates much effective heating of the low-density electron gas. At 1 kV/cm, which corresponds to the range of moderate electric fields, we observe the onset of the formation of the streaming distribution. The DF has an essential anisotropy, and we can see a visible difference between $N_{\|}^{(MC)}(p_{\|})$ and $N_1^{(MC)}(p_1)$. In contrast to shifted Maxwellian form of $N_{\|}^{(B)}(p_{\|})$, $N_{\|}^{(MC)}(p_{\|})$ is non-symmetric. Instead of a rigid displacement of the DF $N_{\|}^{(B)}(p_{\|})$, we observe sprouting the right shoulder of $N_{\|}^{(MC)}(p_{\|})$. It describes the fact that the number of high-energy electrons with the momentum along the field prevails over those with the momentum opposite to the field. The transverse distribution $N_1^{(MC)}(p_1)$ has strictly symmetric form at various fields. The case of 5 kV/cm is close to the developed streaming situation. The longitudinal distribution has a practically step-like shape in the passive region of positive $p_{\|}$ with the right tail that describes weak penetration into the active region. In the model of the infinitely fast emission of the optical phonons, we would obtain an ideal streaming with a constant longitudinal distribution over the whole passive region for $p_{\|} \in [0, p_{LO}]$ at zero longitudinal distribution

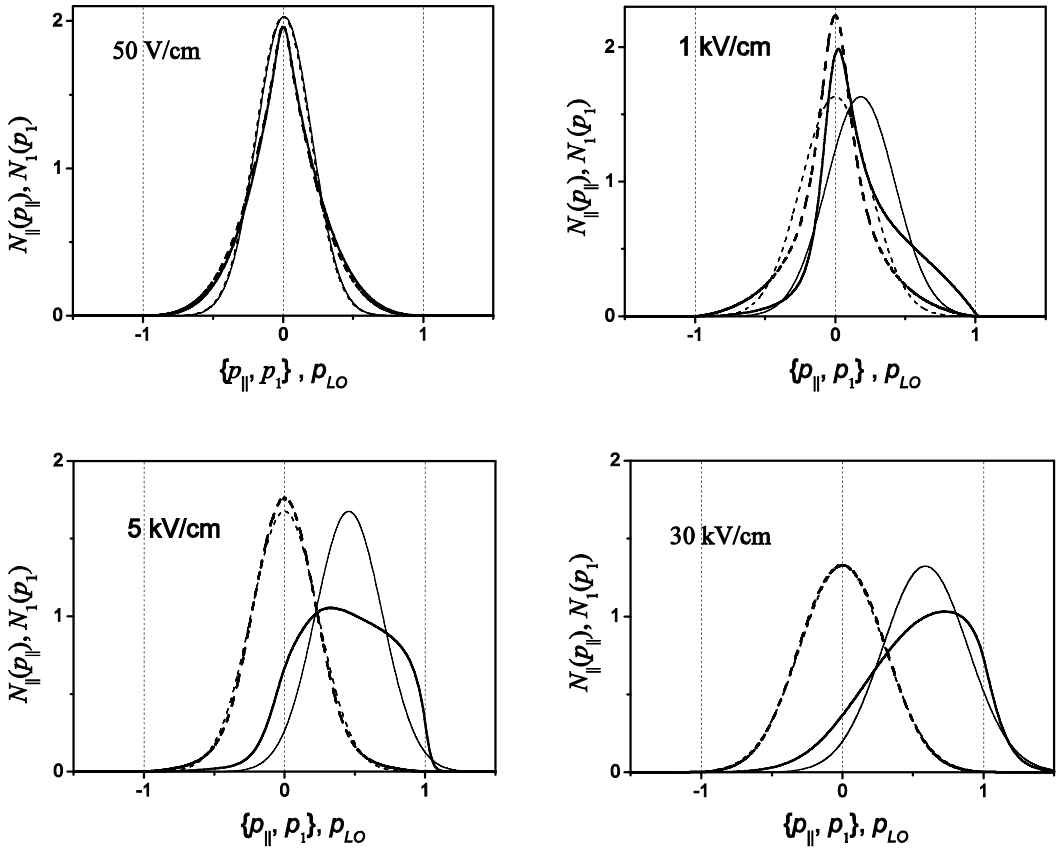

Fig. 8. The longitudinal $N_{\|}(p_{\|})$ and transverse $N_1(p_1)$ electron distributions as functions of momentums $p_{\|}$ and p_1 in units of $P_{LO} = m^* V_{LO}$ at various electric fields. Thick solid and dash lines are the results of MC-simulation for $N_{\|}(p_{\|})$ and $N_1(p_1)$, respectively. Thin lines indicate the results of the BEs approach. T = 77 K.

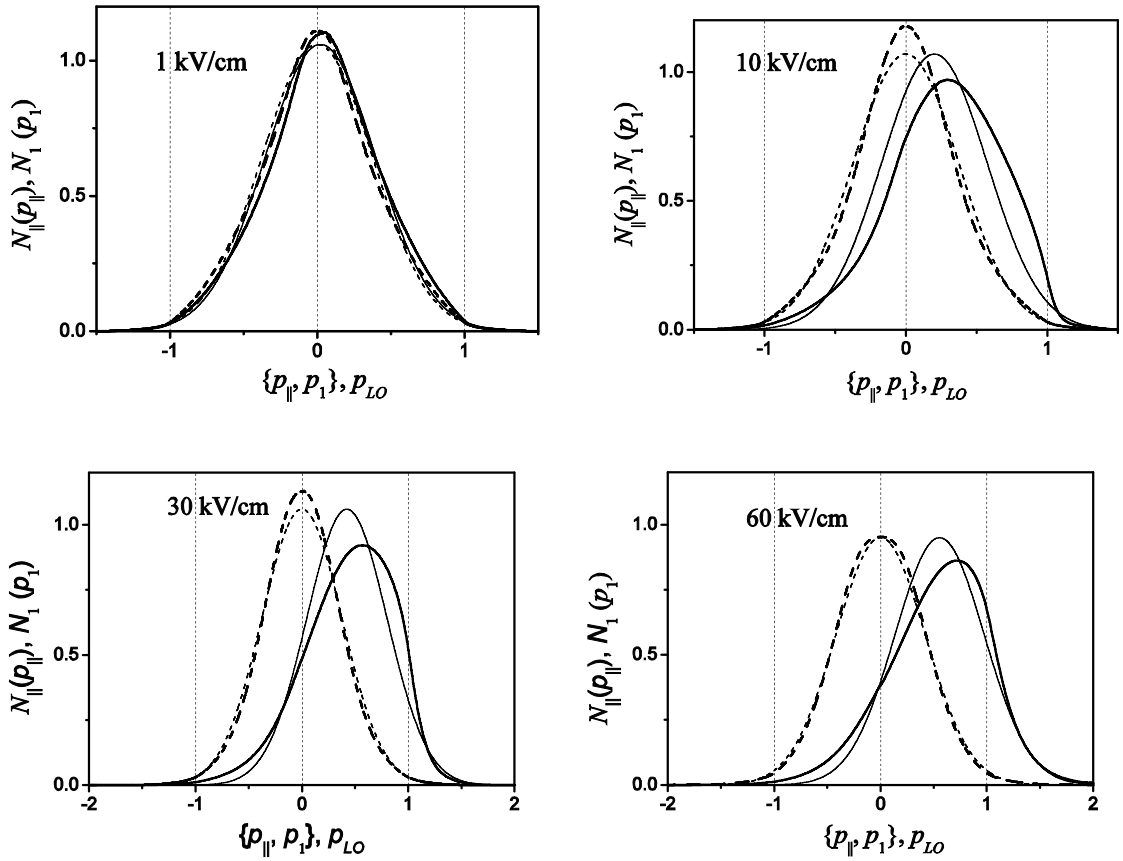

Fig. 9. The longitudinal $N_{\|}(p_{\|})$ and transverse $N_1(p_1)$ electron distributions as functions of momentums $p_{\|}$ and p_1 in units of $P_{LO} = m^* V_{LO}$ at various electric fields. Thick solid and dash lines show the results of MC-simulation for $N_{\|}(p_{\|})$ and $N_1(p_1)$, respectively. Thin lines represent the results of the BEs approach. T = 300 K.

out of this interval. At 30 kV/cm, we observe decay of the streaming regime due to large penetration of electrons into the active region. The longitudinal DF $N_{\|}^{(MC)}(p_{\|})$ gets loss the own step-like shape but keeps the asymmetry.

The situation of room temperature is more prosaic. The longitudinal and transverse distributions are depicted in Fig. 9 for both approaches. At 1 kV/cm for 300 K, both approaches give us practically the same results. The distribution functions are close to the equilibrium Maxwellian form in contrast to the case of nitrogen temperature. The essential deviation from the equilibrium state is observed beginning at about 10 kV/cm. The longitudinal distribution $N_{\|}^{(MC)}(p_{\|})$ shows weak asymmetry instead of the streaming, step-like behavior characteristic for the nitrogen temperature. At higher fields 30, 60 kV/cm, this style of $N_{\|}^{(MC)}(p_{\|})$ is not changed, including stronger penetration into the active region, and similarity to a shifted Maxwellian distribution. Also we note that there are no significant distinctions in the behavior of the longitudinal and transverse distributions and therefore the DF has rather spherical symmetry at different applied fields. Thus, we can conclude that streaming regime is not possible to be achieved at room temperature. In the high temperature case, the both approaches give very similar results for both the DF and the transport characteristics.

5. Conclusions

We have studied the electrical properties of bulk GaN in the frame of two different models corresponding to the low-density and the high-density electron gas. For the first model we used the single-particle MC method which neglects the e-e scattering and the BEs method for the second model. We have investigated the distribution functions, dependences of the drift velocity and the mean electron energy on the applied field in a wide range of fields and temperatures.

We have found the strong dissimilarity between the transport characteristics calculated using the MC and BEs methods in the low-field range (0-1 kV/cm). In GaN, the MC calculation predicts observation of the streaming effect at 77 K at fields of 2-10 kV/cm. We

pointed out that both approaches give the quasi-saturation behavior of $V_d(E)$ at streaming fields. However, the distribution function obtained by the MC-method has a strong anisotropy unlike the shifted Maxwellian distribution function which is caused by the strong e-e scattering. At higher fields (20-80 kV/cm), the streaming effect is destroyed. At fields >80 kV/cm in the frame of the MC-method, the transport characteristics show a superlinear growth that illustrates the onset of runaway. At 300 K the streaming effect is absent. The distribution functions and transport characteristics obtained by the MC-method and BEs one show more similar behavior than at 77 K.

6. Appendix

From the momentum balance equation Eq. (5) in the limit $T_e = T$ and at drift velocity much less than the thermal velocity $V_D << V_T = \sqrt{\frac{2k_BT}{m^*}}$, we obtain mobility:

$$\mu_B = \frac{3\sqrt{\pi}}{4}\frac{e}{m^*}\langle R(\varepsilon)\rangle^{-1}. \qquad (11)$$

In contrast to that case, from the second Eqs (7) and (10), the diffusion approximation gives us another determination of the mobility:

$$\mu_D = \frac{4}{3\sqrt{\pi}}\frac{e}{m^*}\left\langle R(\varepsilon)^{-1}\right\rangle. \qquad (12)$$

In Eqs (11) and (12), $\langle R(\varepsilon)\rangle = (k_BT)^{-5/2}\int_0^\infty d\varepsilon\, \varepsilon^{3/2}R(\varepsilon)\exp\left(\frac{\varepsilon}{k_BT}\right)$ is the statistical average of momentum relaxation rate $R(\varepsilon)$. The mobilities μ_B and μ_D coincide when $R(\varepsilon)$ does not depend from the energy. If we suppose one scattering mechanism with power law of $R(\varepsilon) \sim \varepsilon^s$, then the ratio $\frac{\mu_B}{\mu_D} = \frac{9\pi}{16\Gamma(s+5/2)\Gamma(5/2-s)}$ (where Γ is the Gamma function). For example, for the only acoustic phonon scattering $s = 1/2$ and $\frac{\mu_B}{\mu_d} \sim 0.9$, for the only ionized-impurity scattering $s = -3/2$, and we obtain $\frac{\mu_B}{\mu_d} \sim 0.3$. For a known scattering mechanism, the mobility in high-density electron gas is always less than for the low-density electron gas. In our transport model, we obtain $\frac{\mu_B}{\mu_d} \sim 0.6$ at 77 K. It is also important that Eqs (11), (12) are valid only for the quasi-elastic scattering mechanism.

Acknowledgement

The authors would like to express their gratitude to Professor B.A. Danilchenko for his valuable discussions on various aspects of this work.

References

1. V.E. Gantmakher and Y.B. Levinson, *Carrier Scattering in Metals and Semiconductors*. North-Holland, Amsterdam, 1987.
2. D.K. Ferry, High-field transport in wide-band-gap semiconductors // *Phys. Rev B* **12,** p. 2361-2369 (1975); K.W. Kim, V.N. Sokolov, V.A. Kochelap, V.V. Korotyeyev, and D.L. Woolard, High-speed and high-frequency electron effects in nitride semiconductors for terahertz applications // *Phys. status solidi* (*c*) **2**(7), p. 2569-2572 (2005) (with regard to group III-nitride).
3. W. Fawcett, A.D. Boardman and S. Swain, Monte-Carlo determination of electron transport properties in gallium arsenide // *J. Chem. Solids* **31**, p. 1963 (1970).
4. C. Jacoboni and L. Reggiani, The Monte Carlo method for the solution of charge transport in semiconductors with applications to covalent materials // *Rev. Mod. Phys.* **55**(3), p. 645-705 (1983).
5. H.D. Rees, Calculation of distribution functions by exploiting the stability of the steady state // *J. Phys. Chem. Solids* **30**, p. 643-655 (1969).
6. H. Kosina, M. Nedjalkov, and S. Selberherr, The stationary Monte Carlo method for device simulation. I. Theory // *J. Appl. Phys.* **93**(6), p. 3553-3563 (2003).
7. B. Gelmont, K. Kim and M. Shur, Monte Carlo simulation of electron transport in gallium nitride // *J. Appl. Phys.* **74**, p. 1818-1821 (1993).
8. U.V. Bhapkar and M.S. Shur, Monte Carlo calculation of velocity-field characteristics of wurtzite GaN // *J. Appl. Phys.* **82**, p. 1649-1655 (1997).
9. Sh. Chen and G. Wanga, High-field properties of carrier transport in bulk wurtzite GaN: A Monte Carlo perspective // *J. Appl. Phys.* **103,** 023703 (2008).
10. G.I. Syngayivska and V.V. Korotyeyev, Monte Carlo Simulation of hot electron effects in compensated GaN semiconductors at moderate electric fields // *Semiconductor Physics, Quantum Electronics & Optoelectronics* **10**(4), p. 54-59 (2007).
11. M. Levinstein, S. Rumyantsev, and M. Shur, *Properties of Advanced Semiconductor Materials*: *GaN, AlN, InN, BN, SiC, SiGe* .Wiley, New York, 2001.
12. J.M. Barker, D.K. Ferry, D.D. Koleske and R.J. Shul, Bulk GaN and AlGaN/GaN

heterostructure drift velocity measurements and comparison to theoretical models // *J. Appl. Phys.* **97**, 063705 (2005).

13. B.A. Danilchenko, S.E. Zelensky, E. Drok, S.A. Vitusevich, S.V. Danylyuk, N. Klein, H. Luth, A.E. Belyaev and V.A. Kochelap, Hot-electron transport in AlGaN/GaN two-dimensional conducting channels // *Appl. Phys. Lett.* **85**, p. 5421 (2004).
14. L. Ardaravichius, A. Matulionis, J. Liberis, O. Kiprijanovic, M. Ramonas, L.F. Eastman, J.R. Shealy, and A. Vertiatchikh, Electron drift velocity in AlGaN/GaN channel at high electric fields // *Appl. Phys. Lett.* **83**(19), p. 4038 (2003).
15. V.L. Bonch-Bruyevich and S.G. Kalashnikov, *Semiconductor Physics*. Nauka, Moscow, 1977 (in Russian).
16. D.K. Ferry, *Semiconductors* (Ch. 10). Macmillan, New York, 1991.
17. I.M. Dykman, P.M. Tomchuk, *Transport Phenomena and Fluctuations in Semiconductors.* Naukova Dumka, Kyiv, 1981 (in Russian).
18. R.I. Rabinovich, On galvanomagnetic phenomena under hot-electron energy scattering on optical phonons // *Fizika Tekhnika Poluprovodn.* **3**(7), p. 996-1004 (1969) (in Russian).
19. Z.S. Gribnikov, V.A. Kochelap, Cooling of current carries under scattering of energy on optical phonons // *Zhurnal Eksp. Teor. Fiziki* **58**(3), p. 1046-1056 (1970) (in Russian).
20. L. Varani, J.C. Vaissiere, E. Starikov, P. Shiktorov, V. Gruzinskis, L. Reggiani and J.H. Zhao, Monte Carlo calculations of THz generation in nitrides // *Phys. status solidi* (*a*) **190**(1), p. 247-256 (2002); Monte Carlo simulation of the generation of terahertz radiation in GaN // *J. Appl. Phys.* **89**(2), p. 1161-1171 (2001).
21. J.T. Lu and J.C. Cao, Monte Carlo study of terahertz generation from streaming distribution of two-dimensional electrons in a GaN quantum well // *Semicond. Sci. Technol.* **20**, p. 829-833 (2005); Hot-electron dynamics and terahertz generation in GaN quantum wells in the streaming transport regime // *Phys. Rev. B* **73**, 195326 (2006).